Atmospheric Research 235 (2020) 104693

Contents lists available at ScienceDirect

Atmospheric Research

journal homepage: www.elsevier.com/locate/atmosres

Contrasting frontal and warm-sector heavy rainfalls over South China during the early-summer rainy season

Naigeng Wu[a,b], Xi Ding[c,g], Zhiping Wen[c,d,*], Guixing Chen[c,g], Zhiyong Meng[e], Liangxun Lin[f], Jinzhong Min[a]

[a] Collaborative Innovation Center on Forecast and Evaluation of Meteorological Disasters, Nanjing University of Information Science & Technology, Nanjing 210044, China
[b] Key Laboratory of Regional Numerical Weather Prediction, Institute of Tropical and Marine Meteorology, Chinese Meteorological Administration, Guangzhou 510080, China
[c] School of Atmospheric Sciences, Guangdong Province Key Laboratory for Climate Change and Natural Disaster Studies, Sun Yat-sen University, Guangzhou, China
[d] Department of Atmospheric and Oceanic Sciences & Institute of Atmospheric Sciences, Fudan University, Shanghai 200433, China
[e] Laboratory for Climate and Ocean-Atmosphere Studies, Department of Atmospheric and Oceanic Sciences, School of Physics, Peking University, Beijing 100871, China
[f] Guangdong Provincial Meteorological Observatory, Guangzhou 510080, China
[g] Southern Marine Science and Engineering Guangdong Laboratory (Zhuhai), Zhuhai, China

ARTICLE INFO

Keywords:
Warm-sector heavy rainfall
Frontal heavy rainfall
Monsoon
Land-sea breeze
Diurnal variation
Early-summer rainy season

ABSTRACT

Heavy rainfalls occur frequently during early summer (April–June) over South China, causing severe floods. Using 12 years of hourly rain-gauge data, we identify a large number of regional heavy rainfall events and categorize them into two major types based on the strength of synoptic forcing. It is shown that frontal heavy rainfalls associated with fronts or shear lines mainly occurs over inland regions, whereas warm-sector heavy rainfall under weakly forced synoptic environment is observed in coastal areas. The rainfall maxima of both types tend to form over the low-lying plains or sea surfaces adjacent to windward mountains. Frontal heavy rainfall usually propagates southwards with a cold front, while warm-sector events move relatively slowly and produce coherent patterns of rainfall. The occurrence of warm-sector rainfall increases markedly from April to June in a close association with the onset of summer monsoon, in contrast to frontal rainfall with less monthly variation. Warm-sector rainfall also exhibits pronounced diurnal variation, with a peak in the early morning, as a result of intensified convergence between nocturnal low-level jets in southerly monsoon and land breezes. In contrast, frontal rainfall has an afternoon peak, due to the arrival of eastward-propagating rain systems and daytime heating on land. As frontal (warm-sector) heavy rainfall has relatively high (low) predictability in numerical models, understanding their occurrence and formation is of benefit to operational forecasting and decision-making for disaster prevention.

1. Introduction

Heavy rainfall is one of the most devastating natural disasters over South China during the early-summer (April–June) rainy season, but its prediction remains challenging in operational forecasting and research communities (e.g., Sharma, 2016; Srinivas et al., 2018; Budakoti et al., 2019). The occurrence of heavy rainfalls is affected by synoptic-scale disturbances, mesoscale convective systems (MCSs), boundary-layer processes, and underlying surfaces (Maddox et al., 1979; Heideman and Fritsch, 1988; Schumacher and Johnson, 2005; Caccamo et al., 2017; Wu et al., 2019). Topography and long-term (sub-seasonal-to-seasonal and inter-annual) atmospheric variability are also important to the occurrence of heavy rainfall events over this region (Huang et al., 1986; Chen et al., 2018). The response of heavy rainfalls to various atmospheric conditions and local forcings is key to understanding extreme weather and regional climate over South China. Furthermore, studies on the detailed characteristics of torrential rainfall and related processes help to improve quantitative precipitation forecast, disaster prevention, water resource management, and hydrological research.

Previous studies have shown that heavy rainfall is closely related to the forcings of synoptic-scale weather systems, especially fronts and the activities of the accompanying MCSs (e.g., Glass and Ferry, 1995; Doswell et al., 1996; Junker et al., 1999; and Moore et al., 2003). Maddox et al. (1979) divided heavy rain events caused by non-tropical systems in the eastern United States into three categories: those forced by large-scale weather systems, quasi-stationary fronts in a weak large-

* Corresponding author at: School of Atmospheric Sciences, Sun Yat-sen University, Guangzhou, China.
E-mail address: zpwen@fudan.edu.cn (Z. Wen).

https://doi.org/10.1016/j.atmosres.2019.104693
Received 2 March 2019; Received in revised form 21 September 2019; Accepted 24 September 2019
Available online 31 October 2019
0169-8095/

scale environment, and quasi-stationary cool-air outflow boundaries (gust fronts), respectively. Heavy rainfall events over East Asia during the early-summer rainy season are mainly related to the quasi-stationary meiyu/baiu fronts (Matsumoto, 1971; Ninomiya, 1984, 2000; Ding, 1992; Chen, 2004; Xu et al., 2009; Luo et al., 2013), where the MCSs develop frequently (Kuo and Chen, 1990; Chen, 2004; Zhang et al., 2006). From the perspective of seasonal variation, the early-summer rainy season (April–June) has the maximum number of fronts that affect South China (Ding, 1992). In mid and late June, these fronts (i.e., meiyu/baiu front) mainly appear in central China associated with the northward movement of the summer monsoon. In mid and late July and August, as the summer monsoon continues to move northwards to North China, South China is rarely affected by these fronts.

In addition to the frontal heavy rainfalls (FR) associated with synoptic fronts, we also see so-called warm-sector heavy rainfalls (WR). These WR events occur in weakly forced synoptic environments or in areas far from frontal systems (Huang et al., 1986; Ding, 1994). Warm and humid southerly oceanic flow in the planetary boundary layer is thought to play a key role in the development of MCSs, resulting in the occurrence of WR (Xia et al., 2006; Zhang et al., 2011; Wang et al., 2014; Wu and Luo, 2016). The southerly oceanic flows not only provided the main moisture source for the heavy rainfall (Xia et al., 2006; Huang et al., 2019b), but also contributed to the initiation of convection (Xia et al., 2006; Zhang et al., 2011). MCSs could be maintained by lifting southerly oceanic flows over mesoscale outflow boundary that are enhanced by convectively generated cold pool (Wu and Luo, 2016; Liu et al., 2018; Huang et al., 2019a). Ensemble forecasts of WR (FR) usually have a relatively large (small) spread and a large (small) bias of ensemble-mean amount, suggesting a difference in the predictability for these two kinds of heavy rainfall (Du and Chen, 2018). However, these existed analyses are mainly based on case studies, the climatic characteristics of WR and the comprehensive impacts of multi-scale weather systems are still not clear. Thus far, we have less of an understanding with respect to WR formation than that of FR, meaning the ability to forecast WR events remains limited.

Statistical data in sufficiently large quantities can help towards improving our understanding and prediction of heavy rainfall (Maddox et al., 1979; Schumacher and Johnson, 2005). The climatology of WR and FR events in South China is of particular interest, given that the characteristics and formation of heavy rainfalls events in this region may differ depending on the strength of synoptic forcings. Such studies have become possible with the advent in recent years of long-term observations (Luo et al., 2016). Warm-season rainfall exhibits several regional maxima, often referred to as the 'hotspots' of heavy rainfall in South China. Many analyses have connected the rainfall climatology with the effects of low-level jets (Chen et al., 2018; Du and Chen, 2019), orographic lifting/blocking (Xu et al., 2012; Jiang et al., 2017), urban effects (Wu et al., 2019) and land–sea breezes (Chen et al., 2016; Zhu et al., 2017). However, the impacts of these factors on the occurrence of heavy rainfall under different strengths of synoptic forcing, in particularly for the most frequency WR and FR, remain to be clarified from a climatological perspective.

Rainfall over southeastern China is known for its pronounced diurnal variation (Chen et al., 2009a, 2009b; Chen et al., 2015). Both the daily mean and diurnal amplitude of rainfall intensifies remarkably in early summer. Morning-peak rainfall dominates the windward coasts or mountains, while afternoon-peak rainfall prevails over most inland regions. Recent studies have revealed three modes of rainfall diurnal cycle over southern China: an eastward- or southeastward-propagating mode, a quasi-stationary mode, and an inland-propagating mode (Jiang et al., 2017). The diurnal variation of rainfall anomalies over the south China coastal area during different boreal summer intraseasonal oscillation phases can be interpreted as the interaction between the large-scale anomalous moisture advection and the local land and sea breeze circulations (Chen et al., 2019). The complex diurnal, seasonal, inter-annual and interdecadal trends of inland and coastal precipitation, as well as the relationship between monsoon and land-sea breeze have also been analyzed (Chen et al., 2018). These previous statistical studies, however, have tended to focus on the seasonal variation of rainfall, with the diurnal cycle of heavy rainfall (events) heaving been less well studied.

Using 12 years of hourly rain-gauge data, the present work analyzes the climatology of FR and WR over South China based on a large number of regional heavy rainfall events. Through comparing their characteristics and related atmospheric conditions, we aims to reveal the occurrence and possible mechanisms of these two kinds of heavy rainfalls. Section 2 introduces the data used in this study, the definitions of WRs and FRs, and case statistics. Section 3 compares WR with FR events in terms of their temporal and spatial distributions of rainfall. The differences between WR and FR with respect to their associated atmospheric circulations, as well as their diurnal variations, are presented in Section 4. Finally, Section 5 provides a summary and discussion.

2. Data and methods

2.1. Data

The data used in this work include surface and radiosonde observations in China during April–June of 2003–2014 provided by the China Meteorological Administration. Hourly rainfall and wind observations come from 86 routine surface stations in Guangdong Province of China (110°–117.1°E, 20.3°–25.2°N). These rain-gauge sites are scattered over an area of ~180,000 km^2 at a spatial resolution of ~46 km. Such quality-controlled data can provide a reliable record of rainfall activities at high spatiotemporal resolutions. Considering surface observations cannot measure rainfall over ocean areas, Tropical Rainfall Measuring Mission (TRMM) precipitation data (TRMM-3B42, 3-hourly, 0.25°), which is derived from the TRMM Multi-satellite Precipitation Analysis (Huffman et al., 2007), are also analyzed as an additional source to those based on surface observations. The TRMM data are reasonably reliable for capturing spatial, seasonal, inter-annual and inter-decadal trends in the diurnal variation of precipitation in South China (Chen et al., 2018). The synoptic-scale features of WR and FR are examined using NCEP Final Operational Global Analysis data (6-hourly, 1.0°), which are widely used in weather and climate analyses in China (Luo et al., 2013; Huang and Meng, 2014; Wang et al., 2015; Jiang et al., 2017).

2.2. Definitions of WRs and FRs

Front identification at the surface is important for defining WRs and FRs. Generally, front identification is based on the gradient of ground or low-level meteorological elements. The inclining feature of fronts together with the hilly terrain in South China make objective front identification quite difficult. Therefore, in this paper, the locations of fronts are analyzed by forecasters who subjectively locate fronts using a combination of temperature and wind observations in the surface and 925-hPa layers. Specifically, if a front is strong (clear) enough in the surface analyses, we locate the fronts based on the hourly surface observations (mainly by significant temperature gradients). Otherwise, we determine the fronts mainly based on the 925-hPa directional wind shear (significant difference in wind direction) and temperature gradients.

Meanwhile, considering the possible influence of the spatiotemporal resolution of soundings (twice-per-day observations, four soundings over Guangdong Province) and the hilly terrain of South China on the determination of front position, we define WR as the torrential rainfall that appears > 200 km ahead of the front line (Huang et al., 1986) (Fig. 1a, c). The distance (200 km) from the front line is used to make sure that the rainstorm is not triggered by the synoptic-scale frontal system. FR refers to the torrential rainfall that appears within 200 km

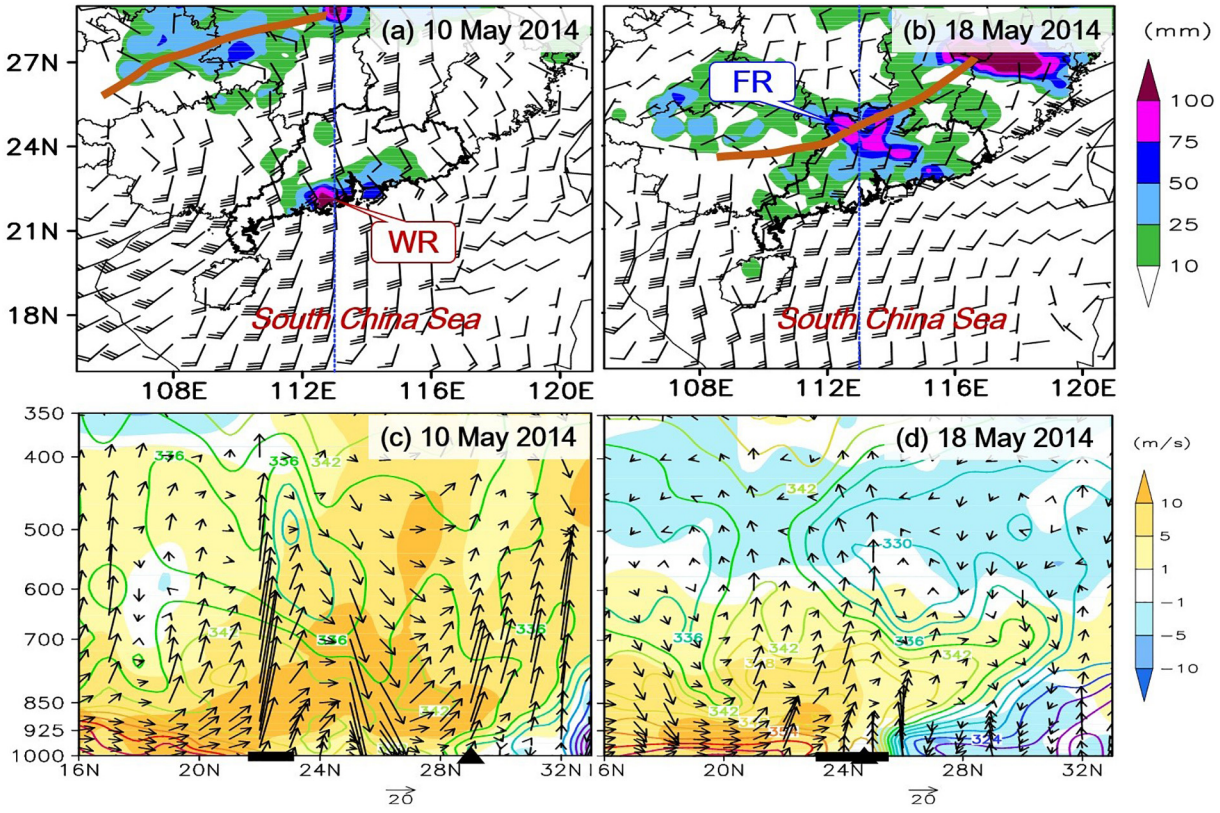

Fig. 1. Distributions of precipitation and the circulation situation at (a, c) 0800 LST on 10 May 2014 and (b, d) 0800 LST on 18 May 2014: (a, b) 925-hPa wind field (each bar represents 4 m/s) and cumulative precipitation in the past 24 h (shaded, mm); (c, d) vertical circulation along 113°E, meridional wind (shaded, m/s) and potential pseudo-equivalent temperature (contoured every 3 K). The solid brown lines and dotted blue lines in (a, b) identify the positions of the shear lines and 113°E, respectively. The solid squares and triangles in (c, d) are the latitudinal position of the precipitation areas and the fronts, respectively. (For interpretation of the references to colour in this figure legend, the reader is referred to the web version of this article.)

from the front (Fig. 1b, d).

This work focuses on the regional heavy rainfall events induced by MCSs and excludes local events due to isolated convection. A regional event is defined if the daily rainfall amount above 50 mm is recorded at five or more adjacent rain gauges. The daily amount is an accumulation during 0000–2400 local standard time (LST = UTC + 8 h), because the rainfall minimum usually occurs at midnight (Chen et al., 2018). Heavy rainfall due to tropical cyclones is excluded. A total of 191 regional events of heavy rainfall are observed during April–June of 2003–2014, with a probability of 15.8% in 1092 days. There are 48 WR-only days, 125 FR-only days, and 18 days of both WR and FR. To compare the characteristics of WR and FR, we focus on the WR-only and FR-only days.

Fig. 2 shows the locations of fronts (925-hPa wind shears) during frontal and warm-sector heavy rains. Fronts exist in the South China region in about 40% (20 out of 48) of WR cases and the locations of all these fronts are far from Guangdong Province (Fig. 2a). In FR, the locations of fronts are more to the south and all of them are located in Guangdong Province (Fig. 2b). However, it should be noted that the classification of heavy rains is based on the relative position of the rainfall and front, rather than the location of the front. Therefore, for different cases of heavy rain in a certain area, the specific location of the front might vary.

3. Spatial pattern and temporal variation of heavy rainfalls

3.1. Spatial distribution of WR and FR

Fig. 3 shows the daily-mean precipitation during the WR and FR days. The spatial distributions differ markedly between the two types of heavy rainfall. The daily mean precipitation centers (exceeding 30 mm/d) of WR days are located in the southwest and southeast coastal areas, with a distance of 50–70 km from the coastline (red solid rectangles in Fig. 3a). Over there, the maximum daily rainfall exceeds 50 mm/d (A, B in Fig. 3a). A secondary maximum of ~40 mm/d is located over the slopes of the mountain range to the northeast of the Pearl River Delta (C in Fig. 3a). By comparison, the area with daily rainfall exceeding 20 mm/d on FR days (shaded) is extensive over Guangdong and much larger than that of WR days (Fig. 3b). The mean rainfall on FR days is evident in central inland areas (blue solid rectangle), with a maximum of > 40 mm (D in Fig. 3b). Overall, WR is mainly confined to coastal areas, whereas FR is spread more inland.

The distribution of daily-mean rainfall based on TRMM data are shown in Fig. 3c and d. The TRMM data reveal a spatial pattern of the daily-mean rainfall that is similar to the rainfall observations (Figs. 3a, b), albeit with an overall smaller magnitude especially for WR. The amount of the WR center in the southwest coastal area is reduced by about 30% (gauge record > 50 mm; TRMM rainfall > 35 mm). This is related to satellite data overestimating the precipitation in the afternoon (probably due to the effect of anvil clouds from afternoon convection on infrared rain estimates), leading to an underestimation of morning precipitation correction (Chen et al., 2018). Coastal precipitation is dominated by morning precipitation and is therefore underestimated more significantly. Despite these errors, satellite data resolve the regional diurnal variations and spatial pattern of rainfall well (Zhou et al., 2008; Chen et al., 2009a, 2018). Moreover, an important feature revealed by the TRMM analysis is that the centers of WR are mainly concentrated near the coastline, which cannot be obtained using observations owing to the lack of stations over the sea.

Fig. 4a and b present the probability of heavy rain (daily

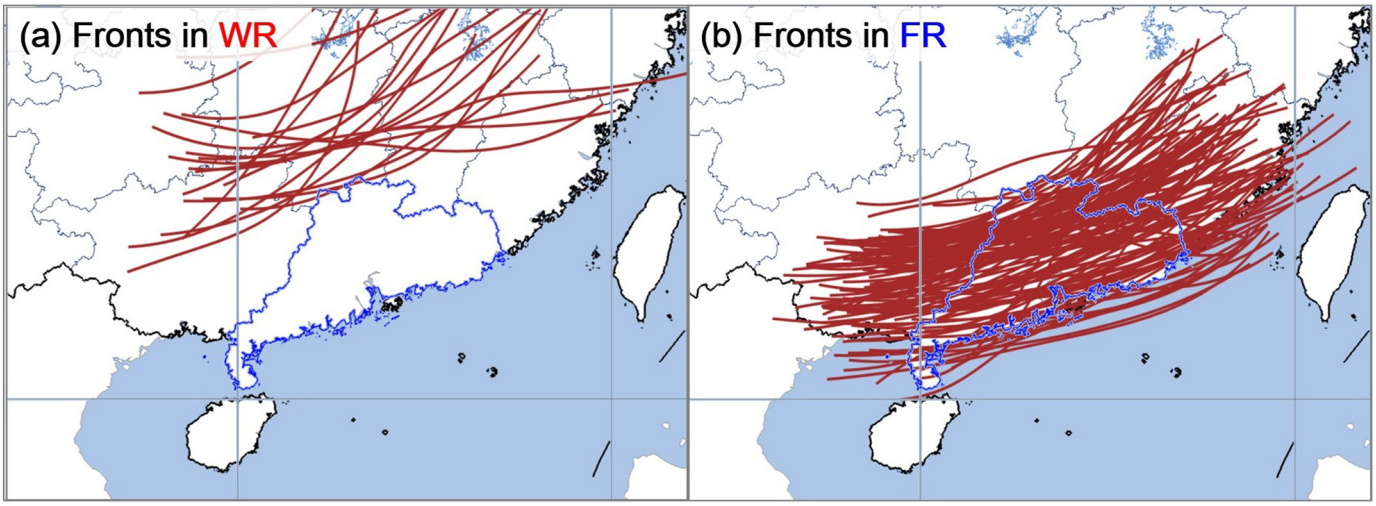

Fig. 2. Locations of the fronts in (a) warm-sector heavy rainfall events and (b) frontal heavy rainfall events.

rainfall > 50 mm) recorded at each station when a WR or a FR event occurs. For WR events, the probability of heavy rain at coastal sites exceeds 40%, which is notably higher than at inland sites (Fig. 4a). This indicates that the occurrence of WR events is concentrated in coastal areas. Similar to Fig. 3a, the maxima of heavy rainfall probability during WR events are located in the southwestern and southeastern parts of coastal areas. Comparatively, the maximum heavy rainfall probability during FR events is relatively low, with a rate of 30% and is located in the central inland area (blue solid rectangle in Fig. 4b).

To further examine the intense rainfall associated with these two kinds of regional events, we estimate the probability of the hourly rain rate exceeding 20 mm/h. Note that, the occurrence of an intense rain rate may be recorded several times at a given site during one event of daily heavy rainfall. Fig. 4c shows that, during WR, there are two maximum centers, located in the southeastern and southeastern parts of coastal areas respectively. The formation of these two precipitation centers is closely related to the coastal mountain terrain (discussed in Section 4). The maximum probability is > 70% in the southwest center and > 60% in the southeast center. In FR, the probability of intense rainfall occurrence in the central inland region is ~40%, but this is much lower than that at the WR centers (Fig. 4d). These patterns in Fig. 4c and d match well with the daily-mean heavy rainfall in Fig. 4a and b. This suggests that WR events are characterized by intense rainfall confined to coastal areas, whereas FR events are characterize by relatively moderate rainfall widespread over the whole region.

To show the initiation location and propagation features of heavy rainfall, we examine the spatial distribution of convective initiation, which is denoted by the first record of the hourly rain rate exceeding 10 mm/h. As shown in Fig. 4e, there are also two maximum centers of convective initiation in coastal areas, which are close to those of the WR centers in Fig. 4a and c. Note that the maximum is about 10%, as an event usually has one record of convective initiation. These features along with the TRMM rainfall (Fig. 3c), show that WR is mainly initiated and grows in coastal areas with windward mountains. Fig. 4f

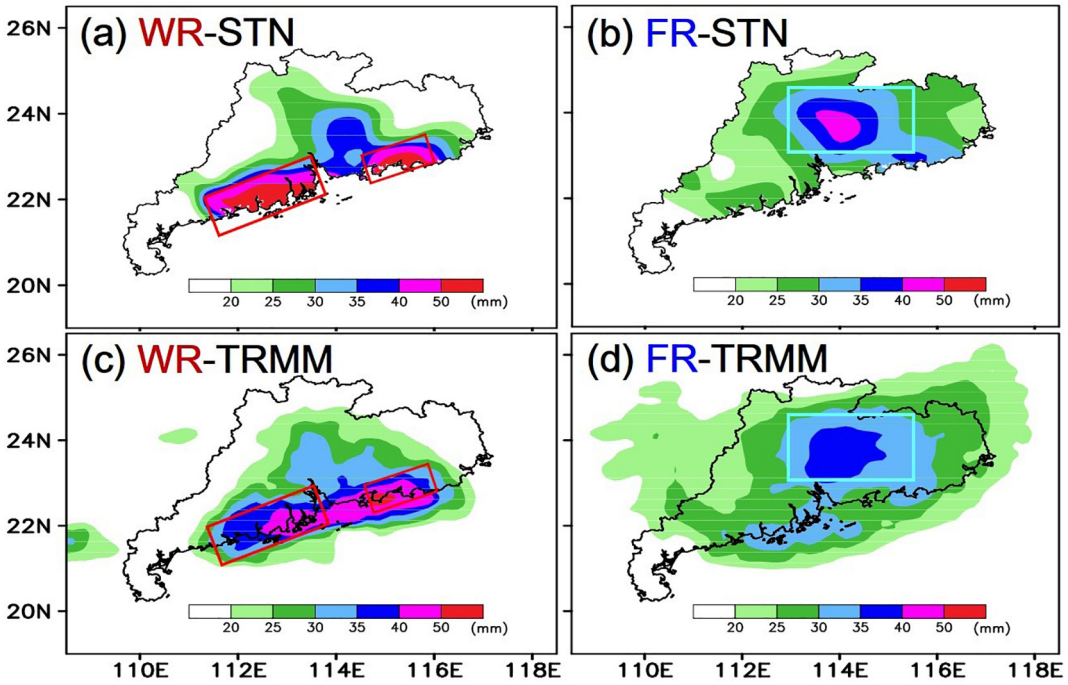

Fig. 3. Daily mean precipitation (shaded, mm) distributions of (a, c) warm-sector torrential rainfall and (b, d) frontal torrential rainfall in the early-summer rainy season from 2003 to 2014, based on (a, b) gauge observations and (c, d) TRMM-3B42 satellite retrieval. Solid rectangles denote the central areas of heavy rainfall.

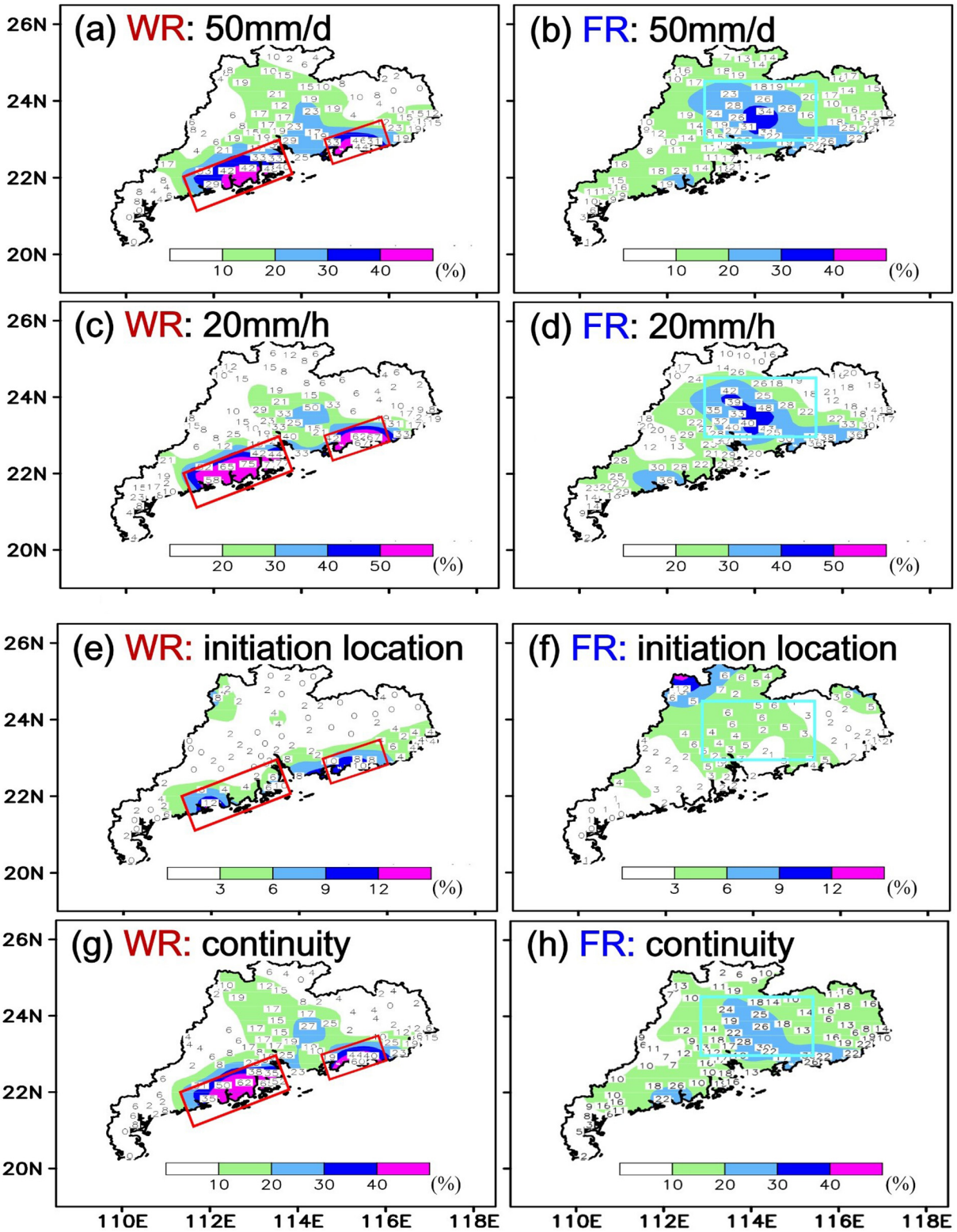

Fig. 4. Distribution of the frequency (%) of heavy rainfall days of (a, c, e, g) WR and (b, d, f, h) FR in the early-summer rainy season from 2003 to 2014: (a, b) daily precipitation ≥ 50 mm; (c, d) hourly precipitation ≥ 20 mm; (e, f) earliest convective precipitation (hourly precipitation > 10 mm) on a heavy rain day; (g, h) hourly precipitation > 10 mm for two consecutive hours.

shows that the earliest convection cells of FR mostly appear at the northwestern border of Guangdong Province, rather than near the rainfall maxima. FR events are thus associated with propagating convective systems associated with fronts from the northwest to southeast.

To further examine the continuity of intense rainfall, we estimate the probability distribution of a rain rate > 10 mm/h for two consecutive hours. As shown in Fig. 4g and h, the maximum centers of WR have a probability of > 60%, which is more than twice that of FRs (20%–30%). This indicates that the convective precipitation of WR is more continuous in time than that of FR. Moreover, results show that

Table 1
Monthly variation of days of WR and FR during April–June from 2003 to 2014.

Days (%)	April	May	June	Total
WR	1 (2%)	13 (27%)	34 (71%)	48 (100%)
FR	31 (25%)	57 (45%)	37 (30%)	125 (100%)

the continuously intense convective rainfall of WR is also mainly concentrated in coastal areas, consistent with the centers of convective initiation in Fig. 4g and accumulated precipitation in Fig. 3a. Therefore, the convective rainfall of WR is more stationary and more likely to produce flash flooding. On the contrary, the continuously intense convective rainfall of FR tends to be scattered, which is consistent with its propagation features associated with fronts.

3.2. Seasonal change and diurnal cycle of WR and FR

In this subsection, we examine the characteristics and possible causes of the monthly variation of WR and FR. Table 1 shows the monthly variation of days of WR and FR during April–June from 2003 to 2014. About 71% of WRs days occur in June, and only one event appears in April. As WR is closely associated with convective precipitation (Section 3.1), its occurrence seems to align with relatively warm and moist conditions. Given the prevailing southwesterly monsoon in June, the associated warm and moist flow may provide favorable conditions for the occurrence of WR. In contrast, FR has a relatively uniform frequency ranging from 25% to 45% during these 3 months. Many previous studies have noted that the major synoptic-scale forcing systems of heavy rains in South China are frontal systems and monsoon flows (Tao and Chen, 1987; Chen, 2009). This means that both cold air from the north and warm air form the south are important for the occurrence of FR. Meanwhile, from April to June, the disturbances of westerly wind (upper westerly troughs and associated cold fronts/shear lines in the boundary layer) exhibit a seasonal weakening. On the contrary, the moisture conditions associated with the South China Sea monsoon show a seasonally enhancement. Thus, the number of FR days is relatively higher (45%) in May when both the westerly wind disturbance in the north and the monsoon activity in the south are stronger.

Previous analyses have noted that the features of the diurnal variations of precipitation in South China vary in different regions and months (Chen et al., 2009a, 2018; Chen et al., 2014b; Jiang et al., 2017). Here, we focus on the diurnal variations related to torrential rain under different synoptic-scale forcing. Fig. 5 shows the spatial distribution of the rainfall peak hour for WR and FR based on surface and satellite observations. The heavy rainfall centers of WR (red solid rectangles in Fig. 5a) tend to peak in the early morning (0500–0900 LST, green arrows). In contrast, the center of FR (blue solid rectangle in Fig. 5b) tends to peak in the afternoon (1200–1800 LST, yellow and red arrows). The TRMM data further reveals that the coastal heavy rainfall of WR is characterized by offshore propagation, while the diurnal phase of the inland heavy rainfalls of FR tends to shift from rainfall in the early morning in the northwest region to the early afternoon rainfall in the southeast region (Fig. 5c, d). The TRMM data thus capture well the diurnal varitations of the two kinds of heavy rainfall well, despite an underestimation of rainfall amount.

We further examine the contribution of diurnally varying heavy rainfall to the seasonal rainfall budget. In the WR center, rainfall increases in the early morning and reaches a peak of about 4 mm/h at 0900 LST (Fig. 6b). Due to the influence of WR (accounts for 20% of total accumulated rainfall in the region during April to June), the climate-mean dirunal cycle in WR center, with a peak at 1100 LST (Fig. 6b), is considerably different to that in other regions of Guangdong Province where the peak is at 1600 LST (Fig. 6d). In contrast, in the FR center, precipitation peaks around noon (1100–1400 LST) and is a little earlier than that of the climate mean dirunal cycle (peak at 1400 LST) in this region (Fig. 6c). Relatively speaking, the FR center exhibits a much smaller dirunal variation (0.8–2.3 mm/h) than that of WR (0.9–3.9 mm/h). Overall, the notable difference between the diurnal cycle modes of WR and FR indicates that their associated physical mechanisms might also be quite different.

4. Physical processes associated with the two kinds of regional heavy rainfall events

4.1. Impact of summer monsoon and frontal activities on WR/FR occurrence

Fig. 7 shows the distribution of dates for heavy rainfall corresponding to WR and FR. WR is found to occur mostly after the onset of the South China Sea monsoon, which generally occurs around mid-May (Fig. 7a). Some cases occur a few days before the monsoon onset date (pentad), which might be related to the definition of the monsoon onset date being based on a large spatiotemporal scale. Actually, before the onset pentad of the South China Sea monsoon, some monsoon surges with a smaller spatiotemporal scale might propagate northwards and affect South China. To further elucidate the impact of southwesterly monsoon flow on WR, the distribution of dates for 850-hPa wind speed and potential pseudo-equivalent temperature (θ_{se}) over the coastal region of South China (112°–116°E, 19°–22°N) are shown (Fig. 8). Clearly, there is a strong correlation between WR and low-level wind speed (Fig. 8a), suggesting that most of the WR appearing in June is closely related to the northward movement of monsoon flow (surges) and convection systems. Meanwhile, the significant increase in warm and wet unstable energy ($\theta_{se} > 340$ K in most cases), which is associated with the northward movement of monsoon, is also critical to the occurrence of WR (Fig. 8b).

For the FR situation, its monthly variation does not have a significant correlation with the onset of the monsoon (Fig. 7b). To demonstrate the impact of fronts on FR, we examine the distribution of dates for 925-hPa meridional wind and relative vorticity over the northern inland area of Guangdong (112°–116°E, 24°–26°N) (Fig. 9). The negative meridional wind and positive relative vorticity depict that the fronts move southward and affect Guangdong. We can see most FR occurs in late-April to mid-June, when frontal activities are the most frequent during the transition from spring to summer. In addition, FR has rarely occurred by the end of June, which corresponds to the strengthening of monsoon flow and northward movement of the rain belt to the Yangtze River (meiyu in central China) (Ding, 1992). Recent studies also suggested that rainfall in South China is closely related with monsoon and westerly wind activities, from the perspective of subseasonal and interannual variations (Chen et al., 2018; Chen et al., 2019).

4.2. Impact of low-level jets and land-sea and mountain–valley breezes on the diurnal variations of heavy rainfall

Fig. 9 shows the composite meridional vertical circulations of WR and FR cases along 113°E. The results show that upward motion is strongest over Guangdong Province in both WR and FR sceniarios. Upward motion during WR is strongest at 21°–23°N, while that during FR is located more to the north at 23°–25°N, which is consistent with the distribution of WR and FR centers. During WR, abundant warm and moist air exists over Guangdong, with the maximum of θ_{se} exceeding 354 K (contours), and southerly airflow dominates the region to the south of 28°N at all levels (Fig. 10a). The upward motion over Guangdong Province (22°–25°N) mainly originates from the low-level southerly that exhibits a strong convergnce of wind speed. In the FR cases, however, the convergence at 22°–25°N is mainly caused by the mid-latitude dry and cold air and the southerly warm and humid airflow from the South China Sea (Fig. 10b). The θ_{se} is about 345–350 K

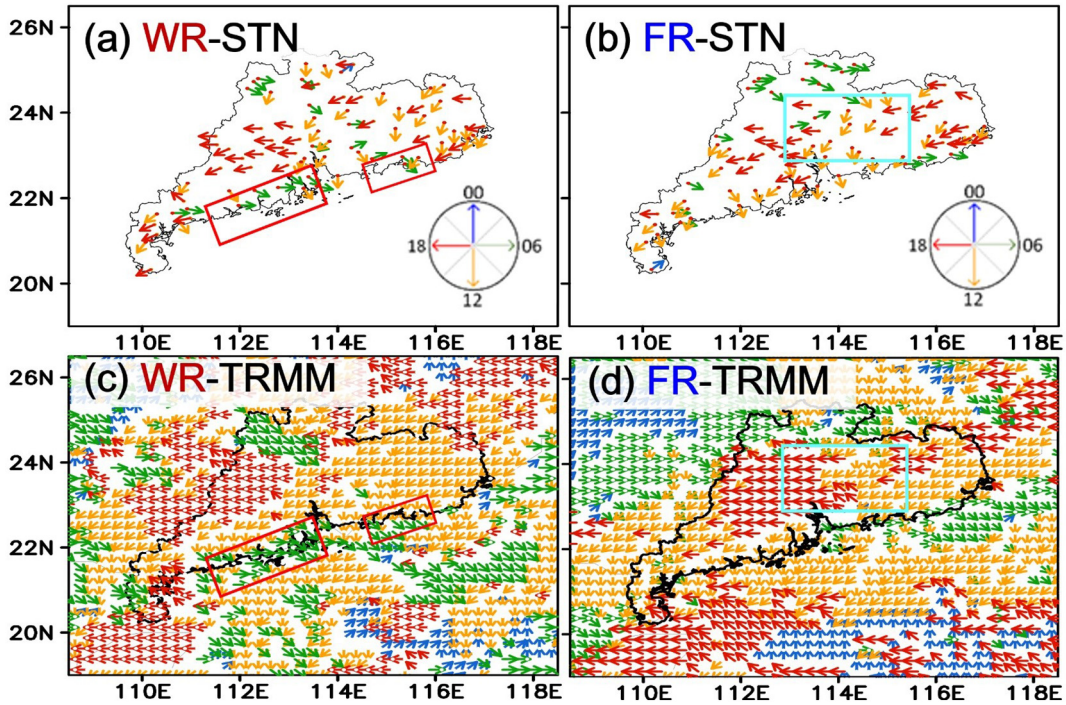

Fig. 5. Distribution of the time of the precipitation peak of (a, c) WR and (b, d) FR in the early-summer rainy season from 2003 to 2014 based on (a, b) rain gauge observations and (c, d) TRMM-3B42 satellite retrieval. The peak value appears northwards at 0000 LST and southward at 1200 LST.

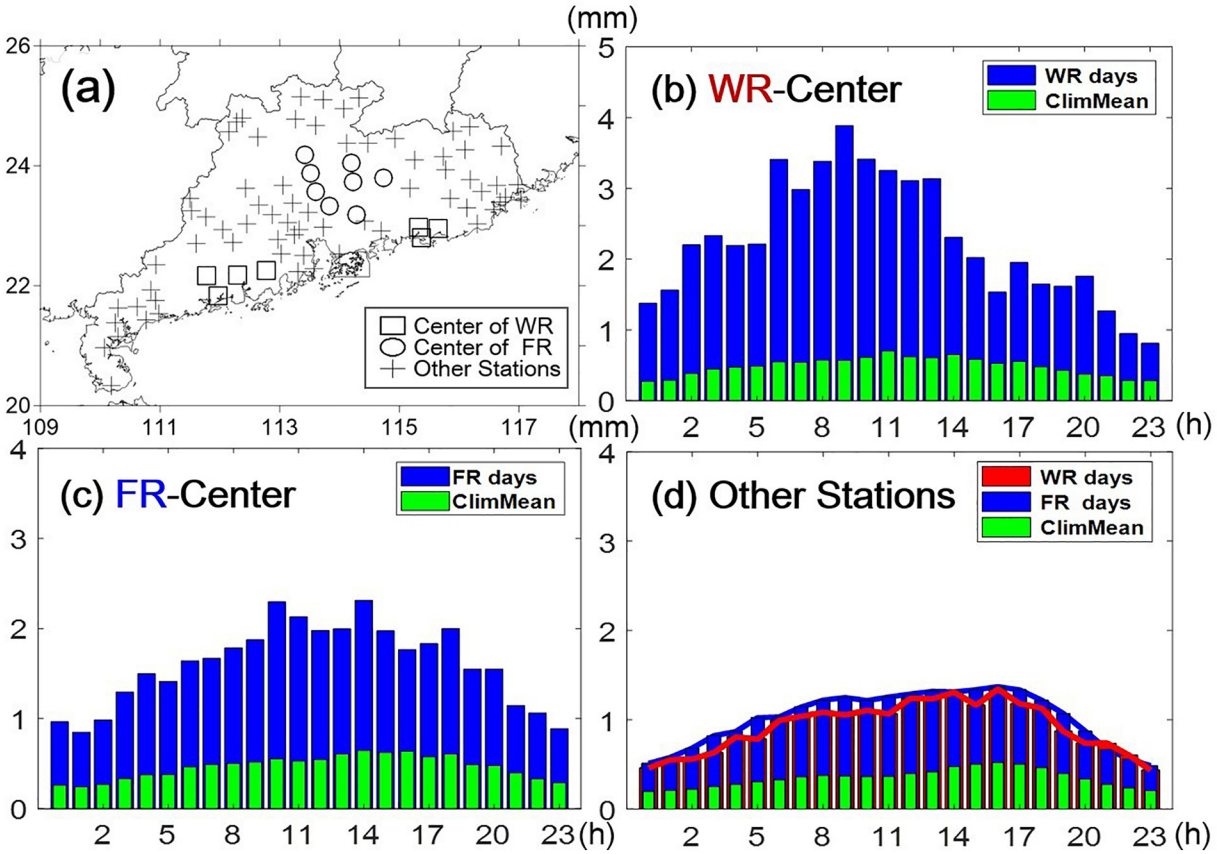

Fig. 6. Diurnal variations of precipitation averaged over stations in the precipitation central areas of (b) WR, (c) FR and (d) other areas in the early-summer rainy season from 2003 to 2014. Panel (a) gives the selection of precipitation central areas. The green histogram shows the evolution of the climate mean. (For interpretation of the references to colour in this figure legend, the reader is referred to the web version of this article.)

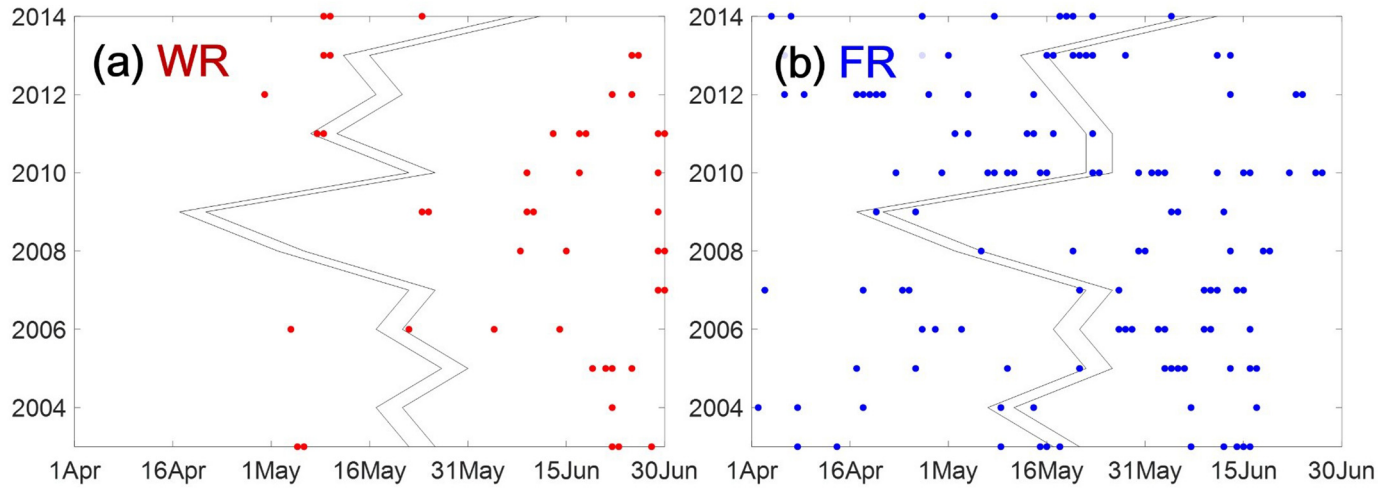

Fig. 7. Distribution of dates for heavy rainfall corresponding to (a) WR and (b) FR. The two solid lines represent the period (pentad) of monsoon onset and the scattered points denote the dates of heavy rainfall occurrence.

over Guangdong, suggesting that the warm and moist air is relatively weaker than that of WR.

In addition, we can see that the vertical centers of southerly warm and humid flow in both the WR and FR cases are located in the boundary layer at 925 hPa rather than at 850 hPa (Fig. 10). Fig. 11 shows the distribution of composite boundary layer wind fields and the temperature field at 925 hPa along with the height of the terrain. Apparently different features of composite winds can be observed at 925 hPa between the WR and FR cases. WR cases mainly occur in an environment with relatively uniform southerly flow (south to southwest) (Fig. 11a). There is no obvious convergence in wind direction or large temperature gradient in South China and the northern part of South China Sea. The maximum wind speed center (112°–114°E, 19°–21°N) appears over the ocean to the south of Guangdong Province and the composite wind speed is larger than 10 m/s with the maximum wind speeds reaching the low-level jet standard of 12 m/s in most (40 out of 48, about 83%) WR cases. The coastal lifting induced by the differential surface friction and small hills may cause strong coastal heavy rainfall on high ambient wind days (Chen et al., 2017). In addition, statistical analysis using reanalysis data makes it difficult to present the small and meso-scale forcing. In contrast, the composite wind based on FR cases has an obvious wind shear and temperature gradient (Fig. 11b) propagating southward. Also, a considerable wind speed center exists over the ocean to the south of Guangdong Province, but its' westerly wind component is larger than that of WR.

To further investigate the relationship between low-level wind and the diurnal variations of heavy rainfall, we analyze the temporal evolution of the low-level wind over the South China Sea. Figs. 12 and 13 show the distribution of the peak/valley times of low-level wind over the South China Sea and the evolution of the precipitation/wind anomaly averaged over the heavy rainfall centers, respectively. The results show that the southerly wind at 925 hPa is strongest at 0200 LST in the WR cases (> 10 m/s) (Figs. 12a and 13a). This is probably related to the notable morning WR peaks through abundant moisture supply and wind speed convergence near the coastal area (Fig. 11a). This result is consistent with previous studies reporting that low-level airflow in the monsoon region tends to strengthen from late afternoon to early evening and contribute to strengthened morning precipitation in coastal areas (Nitta and Sekine, 1994; Terao et al., 2006; Chen et al., 2009a). For FR, the southwesterly low-level airflow is relatively weaker than that during WR (Fig. 13b). The low-level southwesterly slowly increases in the morning and reaches its peak at 1400 LST which is probably associated with the weak afternoon peak of FR. In addition, the considerable attenuation of the southerly winds at 2000 LST in

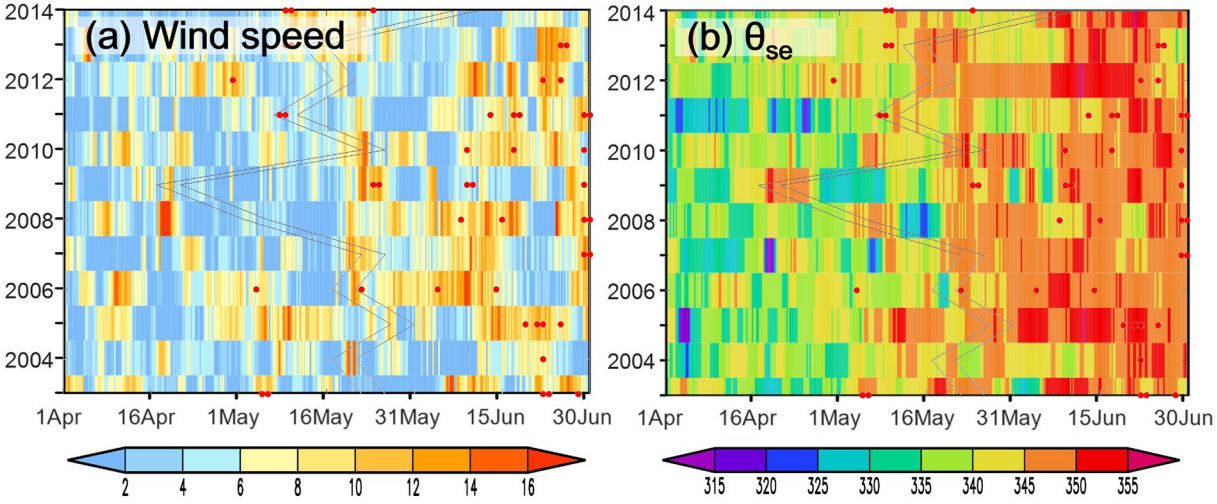

Fig. 8. Distribution of dates for (a) 850-hPa wind speed (shaded, m/s) and (b) potential pseudo-equivalent temperature (θ_{se}, shaded, K) over the coastal region of Guangdong (112–116°E, 19–22°N). The wind speed in (a) is set to a negative value if the meridional wind < 0 m/s (the display colour is consistent with the wind speed threshold < 2 m/s). Two solid lines represent the period (pentad) of monsoon onset and scattered points denote the date heavy rainfall occurs.

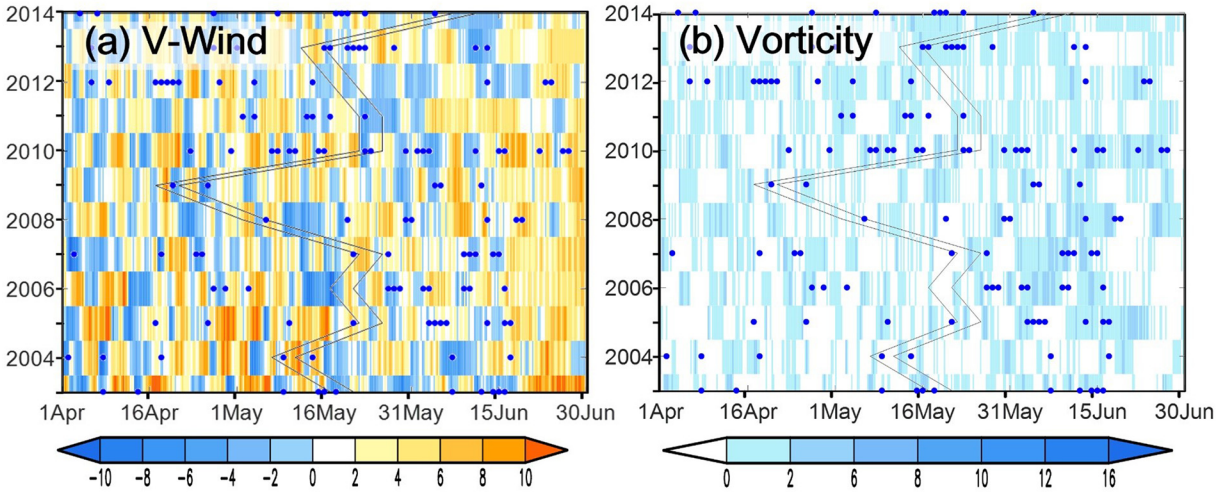

Fig. 9. Distribution of dates for (a) 925-hPa meridional wind (shaded, K) and (b) relative vorticity (positive shaded, 10^{-5}) over the northern inland area of Guangdong (112–116°E, 24–26°N). The two solid lines represent the period (pentad) of monsoon onset and the scattered points denote the dates of heavy rainfall occurrence.

Fig. 13b is likely related to the southward movement of the frontal system (associated with a short-wave trough and northerly wind) to the coast.

Besides the diurnal variation of monsoon flows, the daily variations of heavy precipitation are also associated with land–sea breeze activities. A more apparent diurnal variations in land–sea breezes is observed in WR cases than in FR cases (Fig. 13). In the WR cases, land breezes start to intensify at 0200 LST in the early morning, becoming strongest between 0500 and 0800 LST, which collocates well with peak WR. As offshore land breezes and the onshore monsoon strengthen the convergence at night, the precipitation near the coastal region develops rapidly in the middle of the night to the morning. After 0800 LST, the land breeze weakens and the sea breeze gradually intensifies before peaking in midafternoon. The peak FR, however, bears no significant correlation with the land–sea breezes. These statistical results, from the observational and statistical perspective, confirm the important role of land–sea breezes proposed by previously based on the results of idealized experiments (Chen et al., 2016, 2017) and further reveal that impact of land–sea breezes to precipitation mainly occurs in WR.

To further examine the interaction between onshore monsoon and offshore land breeze, we analyze the local meridional vertical circulation. Fig. 14 shows the meridional vertical circulation difference (that at 0200 LST and 0800 LST minus that at 1400 LST and 2000 LST) of WR and the climate mean along 112°E. For WR, we can find see that southerly winds in the boundary layer strengthen markedly in the early morning, extending northwards and upwards. Meanwhile, temperatures near the surface over land have a maximum absolute difference of > 2 °C, resulting in considerable northerly land breezes on the north side of the coastal line (Fig. 14a). The southerly airflow over the sea and the land breeze over the land result in apparent convergence and this upward motion near the coastline plays an important role in the strengthening of WR in the early morning. In addition, we also find that land breezes occur in the climate mean situation, albeit a little weaker (Fig. 14b). Therefore, the occurrence of WR is closely related to the diurnal variations of large-scale monsoon flow and local land–sea breezes. Relatively speaking, nighttime strengthening of monsoon flow might be the more important factor leading to the frequent occurrence of WRs in early summer in South China.

It is worth noting that the diurnal variations of winds and moisture derived from reanalysis data are probably not as reliable as one might hope. This is because, on the one hand, the mesoscale circulation of diurnal cycles cannot be adequately resolved in the current GFS data assimilation system with its coarse grid spacing and hydrostatic dynamical core; while on the other hand, they are available only four times a

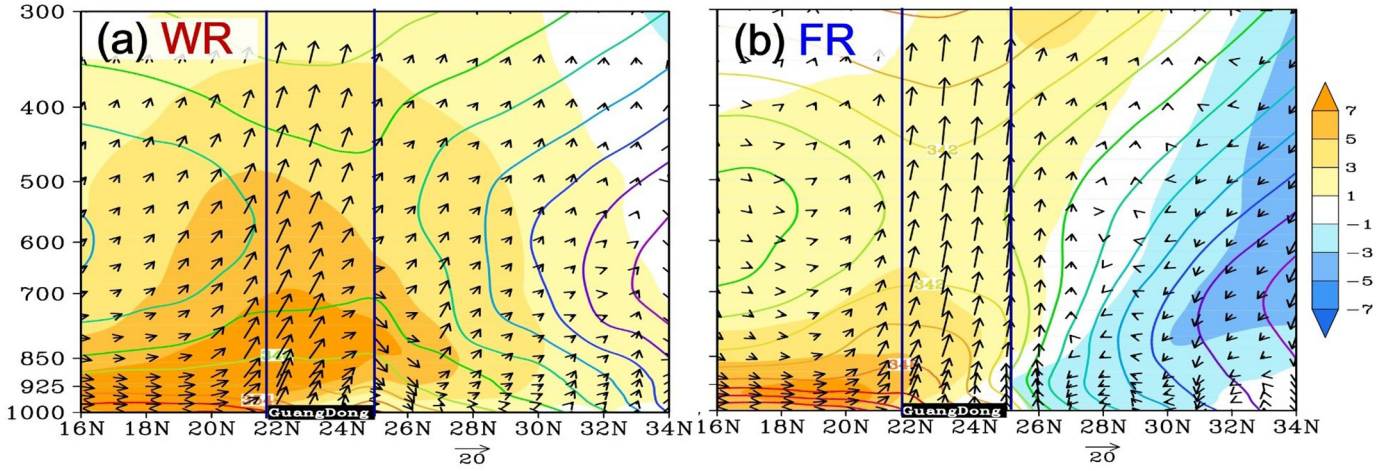

Fig. 10. Composite vertical circulation (wind vectors) and potential pseudo-equivalent temperatures (contoured every 3 K) along 113°E during (a) WR and (b) FR. Shading denotes the meridional absolute wind speed > 1 m/s. Vertical velocity is multiplied by 100 (unit: 0.01 Pa/s). The black frame represents the latitudinal range of Guangdong Province.

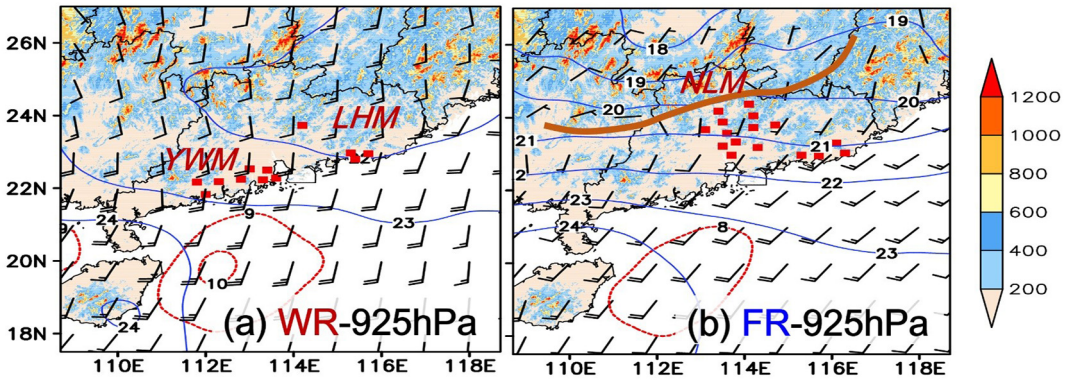

Fig. 11. Distribution of composite low-level wind at 925 hPa (full bar represents 4 m/s, half bar represents 2 m/s, and the red dashed line represents the center of the wind speed), temperature (blue solid line, °C), and terrain height (shaded, m) of (a, c) WR and (b, d) FR. Red squares denote the stations of heavy rainfall centers. NLM, YWM, and LHM denote the Nanling Mountains, Yunwu Mountains and Lianhua Mountains, respectively. (For interpretation of the references to colour in this figure legend, the reader is referred to the web version of this article.)

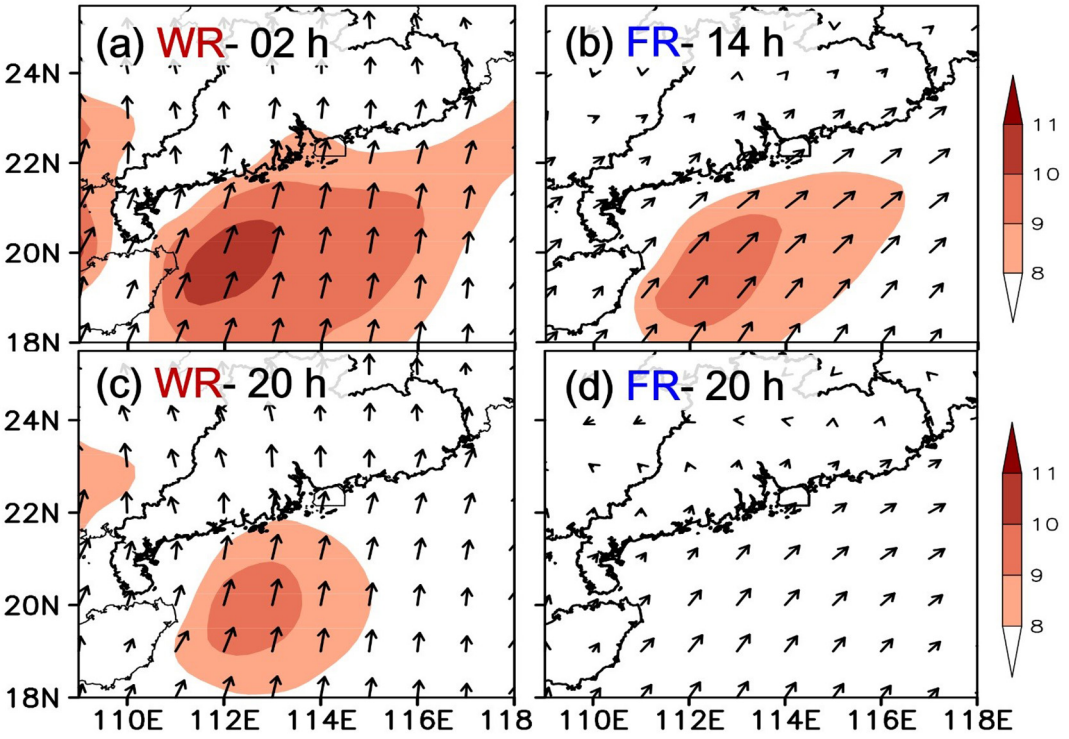

Fig. 12. Distribution of diurnal variations of mean low-level wind at 925 hPa corresponding to (a, c) WR and (b, d) WR: (a, b) peak time of low-level wind over the South China Sea; (c, d) valley time of low-level wind over the South China Sea. Areas with wind speed > 8 m/s are shaded.

day in the reanalysis. Chen et al. (2014a, 2014b) suggested that most mainstream reanalysis data can represent the large-scale features of diurnal cycles over East Asia well, but they suffer from some biases at regional scales (Chen et al., 2014a, 2014b). Studying the diurnal cycles of atmospheric variables associated with heavy rainfall at both regional and large scales would be a valuable future research topic.

4.3. Impact of mountains

Section 4.2 showed that WR occurs more frequently on the windward slopes of the coastal mountains, which is likely related to the effects of the local terrain. To further investigate this, the spatial pattern and diurnal variation of WR are shown based on high-density regional automatic precipitation observations over the southwest coastal mountains (the most prominent center of WR). Fig. 15 shows that WR mainly occurs at the coastline in the early morning (0200–0800 LST) and then shifts to the upslope of inland mountains in the afternoon (1400–2000 LST). Meanwhile, the rainfall in the afternoon has a larger extent but the intensity is lower than that observed in the early morning. Combined with the previous analyses in Sections 4.1 and 4.2, this feature of WR could be because of the interaction between orography and land–sea breeze and low-level monsoon flow. With the strengthening of the southerly monsoon at night, the southerly airflow expands substantially to the north and to a higher level (Figs. 12 and 14). In the meantime, temperatures over land and the mountains decreases, resulting in the northerly land breezes and mountain breezes on the seaward slope of the piedmont.

Based on the above analysis, conceptual model of diurnal variation during WR is summarized in (Fig. 16). Northerly land and mountain breezes converge with strong southerly monsoon airflow at the coastline, resulting in development of strong convection near the coastline in the early morning (Fig. 16a). In the afternoon, however, the southerly

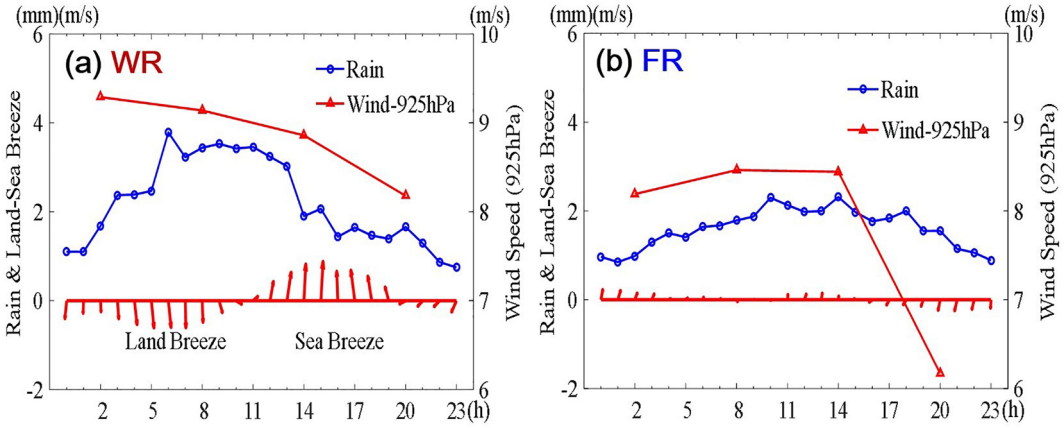

Fig. 13. Diurnal variations of precipitation (solid blue line with circles) and wind (red arrows) averaged over the center gauge stations of (a) WR and (b) FR and the corresponding low-level wind at 925 hPa (solid red line with triangles) over the northern part of the South China Sea [(a) 111–113°E, 18–22°N; (b) 112–114°E, 18–22°N] based on NCEP-FNL analysis data. The selection of center stations is shown in Fig. 5 and the southwest center is represented as WR here considering the spatial discontinuity of the wind. (For interpretation of the references to colour in this figure legend, the reader is referred to the web version of this article.)

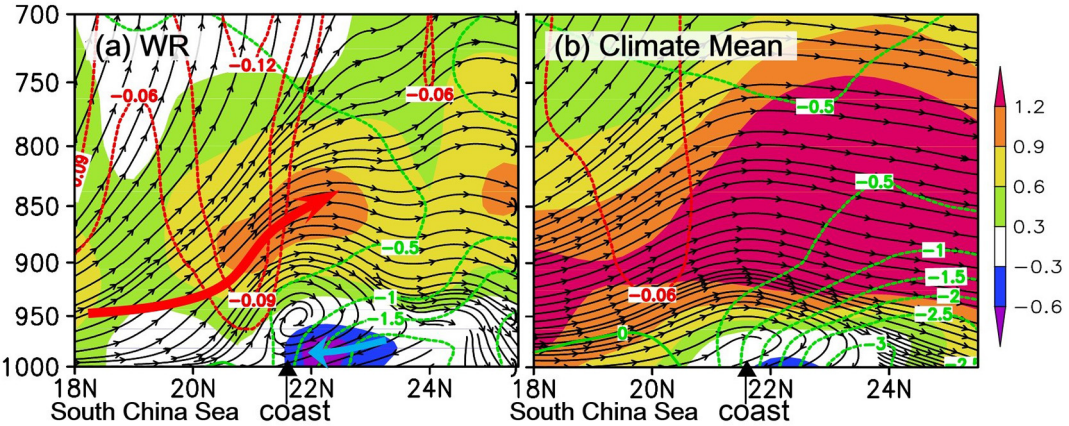

Fig. 14. The meridional vertical circulation difference (that at 0200 LST and 0800 LST minus that at 1400 LST and 2000 LST) of (a) WR and (b) the climate mean (May and June) along 112°E. The shading represents the meridional wind in m/s. The green dotted lines represent the temperature in °C. The red dotted lines represent omega in Pa/s. The vertical movement in stream line is multiplied by 10. The triangle represents the latitude of land along the coast. (For interpretation of the references to colour in this figure legend, the reader is referred to the web version of this article.)

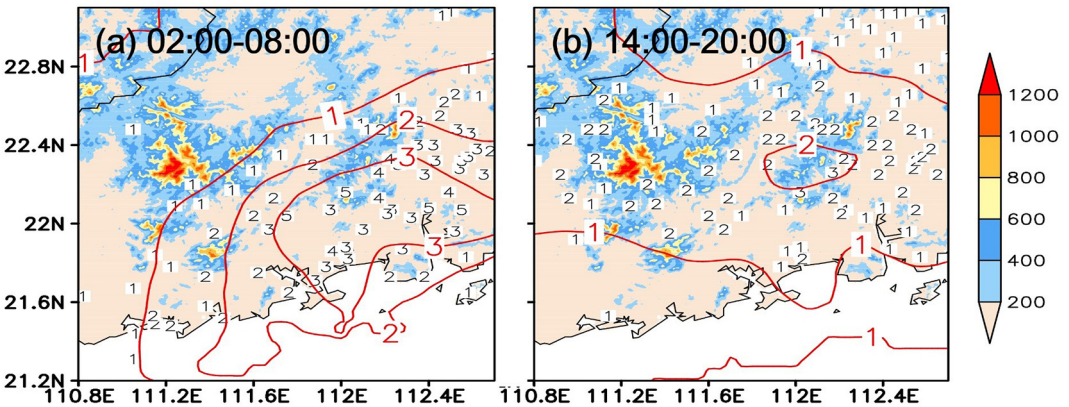

Fig. 15. Distribution of hourly precipitation observations (numbers and contours, mm) from the intensive precipitation stations (a) in the early morning (0200–0800 LST) and (b) in the afternoon (1400–2000 LST) in the central area of warm-sector heavy rainfall events averaged during 2009–2014. The colour shading denotes the terrain height (units: m).

monsoon flow weakens. The land and mountain breezes near the ground change into southerly sea and valley breezes. The joint development of sea breeze and valley wind during the day leads to convection that tends to propagate inland. As a result, convection gradually shifts to the upslope of inland mountains rather than at the coastline (Fig. 16b). The precipitation intensity is lower than that in the early morning likely because of the weakened southerly monsoon airflow during the daytime (Figs. 11c and 13a). Recently, based on idealized numerical experiments, Chen et al. (2016, 2017) revealed the important influences of the prevailing monsoon wind speed (high-wind days and

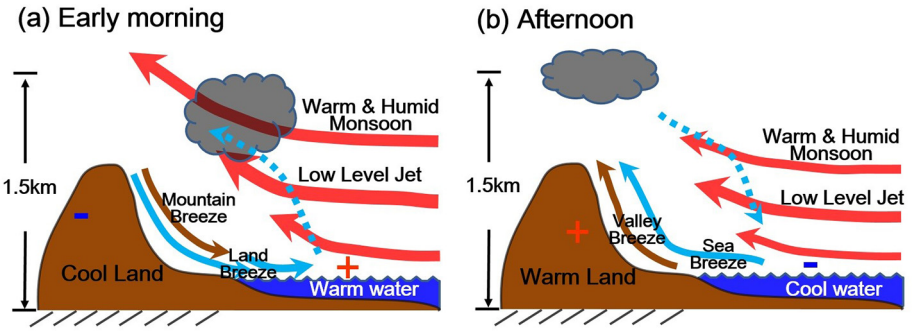

Fig. 16. Schematic diagrams of the influence of land–sea breezes, boundary layer circulation and coastal orography on WR in the (a) early morning and (b) afternoon.

low-wind days) combined with land–sea breeze variation on the diurnal cycle of coastal precipitation over South China. The conceptual model of WR diurnal variation based on statistical observations in this paper, on the one hand, it shows that high-wind-days results of the idealized experiments conducted by Chen et al. (2016, 2017) are more applicable in WR; on the other hand, it further demonstrates the crucial impact of the diurnal variability of both monsoon wind speed and vertical structure. Besides, this conceptual model further reveals the relationship between formation/evolution of WR and the diurnal variability of multi-scale land-sea effects (synoptic-scale monsoon flow and local land-sea breeze) and local orographic effect (lifting/blocking and mountain-valley breeze).

5. Summary and discussion

In the early-summer rainy season, heavy rain events can occur frequently over South China under either strong or weak synoptic forcings, referred to in this paper as FR and WR respectively. Different from previous case studies, this work examines the statistical characteristics and physical processes of FR/WR based on a large number of regional heavy rain events. The major findings can be summarized as follows:

(1) The precipitation centers of WRs and FRs are located in coastal and central inland areas, respectively. Compared with FR, WR has a more obvious continuity of heavy precipitation (slower movement) and a more obvious seasonal variation. For WR, 71% of events occur in June, mainly after the onset of the South China Sea monsoon. The variation of FRs during April–June has a relatively uniform frequency and is not apparently correlated with the onset of monsoon. WR is dominated by southerly wind system, whereas the environments of FR are dominated by northern frontal associated systems and thus propagate faster than WR.

(2) The diurnal signals are usually stronger under weaker synoptic forcings (i.e., WR). WR centers mainly appear in the early morning in the southwest and southeast coastal areas. They are mainly initiated in the coastal areas by the convergence between the strong and deep southerly warm–humid monsoon airflow from the South China Sea and the local land/mountain breezes at night and in the early morning. In the afternoon, WR occurs slightly more inland over the seaward slope of mountains because of the replacement of land/ mountain breezes with sea/valley breezes and their uplifting by the mountains. The peak of FR mainly appears in the afternoon and at dusk, usually initiated in northern Guangdong Province because of the convergence between the mid-latitude northerly dry–cold air and the southerly low-level warm–humid airflow from the South China Sea. There is no obvious correlation between the diurnal variation of precipitation and land–sea breezes.

The results presented in this paper advance our understanding of the occurrence mechanism of heavy rainfall in the tropical monsoon region, where the ability to forecast precipitation is still not high. However, it should be noted that the occurrence mechanism of heavy rainfall, in particularly for the WR, are highly complicated. These statistical results are mainly focus on the thermal-dynamic circulation of the boundary layer and the data resolution is still relatively coarse. It is therefore necessary to carry out cloud-resolving numerical simulation to uncover more details of the physical processes involved, e.g. urban effect (Wu et al., 2019; Huang et al., 2019a), local land-sea effect (Chen et al., 2017) and local orographic effect (Chen et al., 2017; Huang et al., 2019a). The cloud microphysical characteristics of different types of heavy rainfall cases are also should be conducted for future investigation in combination with scientific observation data (Erlingis et al., 2018; Mohan et al., 2018; Patade et al., 2019). These efforts are very important to the evaluation and improvement of numerical weather/climate prediction models.

The predictability of warm-sector heavy rainfall under weak synoptic forcing is a crucial issue. As we know, the predictability of convective weather events are highly flow-dependent (Johnson et al., 2014; Nielsen and Schumacher 2016). Different from the heavy rainfall in the mid-latitudes which is associated with strong baroclinicity or strong synoptic-scale forcing, heavy-rain-producing systems and associated MCSs in the tropical monsoon region usually possess strong convective/conditional instability but weak baroclinicity. Thus far, little is known about the predictability of heavy rainfall in this region (with strong moist convection), especially the frequent flash-flood-producing WR. Further studies of nonlinear error growth dynamics and error sources of NWPs are needed to provide deeper understanding about the intrinsic and practical predictability of different types of heavy rainfall (Melhauser and Zhang, 2012; Bachmann et al., 2019). These efforts are also crucial to the design and implementation of the convection-allowing ensemble forecast systems (Schumacher and Davis, 2010; Melhauser and Zhang, 2012).

Declaration of competing interest

The authors declare that they have no known competing financial interests or personal relationships that could have appeared to influence the work reported in this paper.

Acknowledgements

TRMM 3B42 product data were obtained from the NASA Goddard Earth Science Data and Information Services Center. NCEP FNL analysis data were provided by the National Center for Atmospheric Research via http://rda.ucar.edu/datasets/ds083.2/. This work was jointly supported by National Key Research and Development Program of China (2018YFC1507400, 2017YFC1502103), the National Natural Science Foundation of China (41705035, 41461164006, 41575068), and the Science and Technology Planning Project of Guangdong Province, China (2017A020219005, 2017B020244002). We also thank the anonymous reviewers for their helpful comments towards improving the original version of this paper.

References

Bachmann, K., Keil, C., Craig, G.C., Weissmann, M., Welzbacher, C.A., 2019. Predictability of deep convection in idealized and operational forecasts: effects of radar data assimilation, orography and synoptic weather regime. Mon. Weather Rev. https://doi.org/10.1175/MWR-D-19-0045.1. in press.

Budakoti, S., Singh, C., Pal, P.K., 2019. Assessment of various cumulus parameterization schemes for the simulation of very heavy rainfall event based on optimal ensemble approach. Atmos. Res. 218, 195–206.

Caccamo, M.T., Castorina, G., Colombo, F., Insinga, V., Maiorana, E., Magazù, S., 2017. Weather forecast performances for complex orographic areas: impact of different grid resolutions and of geographic data on heavy rainfall event simulations in Sicily. Atmos. Res. 198, 22–33.

Chen, G.T.-J., 2004. Research on the phenomena of Meiyu during the past quarter century: an overview. In: Chang, C.P. (Ed.), East Asian Monsoon, Vol. 2, World Scientific Series for Meteorology of East Asia. World Scientific, pp. 357–403.

Chen, Y.L., 2009. Some synoptic-scale aspects of the surface fronts over South China during TAMEX. Mon. Weather Rev. 121, 50.

Chen, G., Sha, W., Iwasaki, T., 2009a. Diurnal variation of precipitation over southeastern China: spatial distribution and its seasonality. J. Geophys. Res. 114, D13103.

Chen, G., Sha, W., Iwasaki, T., 2009b. Diurnal variation of precipitation over southeastern China: 2. Impact of the diurnal monsoon variability. J. Geophys. Res. 114, D21105.

Chen, G., Iwasaki, T., Qin, H., et al., 2014a. Evaluation of the warm-season diurnal variability over East Asia in recent reanalyses JRA-55, ERA-Interim, NCEP CFSR, and NASA MERRA. J. Clim. 27 (14), 5517–5537.

Chen, X., Zhao, K., Xue, M., 2014b. Spatial and temporal characteristics of warm season convection over Pearl River Delta region, China, based on 3 years of operational radar data. J. Geophys. Res. Atmos. 119, 12,447–12,465.

Chen, X., Zhao, K., Xue, M., 2015. Radar observed diurnal cycle and propagation of convection over the Pearl River delta during mei-yu season. J. Geophys. Res. Atmos. 120 12 557–12 575.

Chen, X., Zhang, F., Zhao, K., 2016. Diurnal variations of the land–sea breeze and its related precipitation over South China. J. Atmos. Sci. 73, 4793–4815.

Chen, X., Zhang, F., Zhao, K., 2017. Influence of monsoonal wind speed and moisture content on intensity and diurnal variations of the Mei-yu season coastal rainfall over South China. J. Atmos. Sci. 74, 2835–2856.

Chen, G., Lan, R., Zeng, W., 2018. Diurnal variations of rainfall in surface and satellite observations at the monsoon coast (South China). J. Clim. 31, 1703–1724.

Chen, X., Zhang, F., Ruppert, J.H., 2019. Modulations of the diurnal cycle of coastal rainfall over South China caused by the boreal summer intraseasonal oscillation. J. Clim. 32, 2089–2108. https://doi.org/10.1175/JCLI-D-18-0786.1.

Ding, Y., 1992. Summer monsoon rainfalls in China. J. Meteorol. Soc. Jpn 70, 373–396.

Ding, Y., 1994. Monsoons over China. Adv. Atmos. Sci. 11, 252.

Doswell, C.A.I., Brooks, H.E., Maddox, R.A., 1996. Flash flood forecasting: an ingredients-based methodology. Weather Forecast. 11, 560–581.

Du, Y., Chen, G., 2018. Heavy rainfall associated with double low-level jets over 679 Southern China. Part I: ensemble-based analysis. Mon. Wea. Rev. 146, 3827–3844.

Du, Y., Chen, G., 2019. Climatology of low-level jets and their impact on rainfall over southern China during early-summer rainy season. J. Clim. https://doi.org/10.1175/JCLI-D-19-0306.1. in press.

Erlingis, J.M., Gourley, J.J., Kirstetter, P., Anagnostou, E.N., Kalogiros, J., Anagnostou, M.N., Petersen, W., 2018. Evaluation of operational and experimental precipitation algorithms and microphysical insights during IPHEx. J. Hydrometeorol. 19, 113–125. https://doi.org/10.1175/JHM-D-17-0080.1.

Glass, F.H., Ferry, D.L., 1995. Characteristics of heavy precipitation events across the mid-Mississippi Valley during the warm season: meteorological conditions and conceptual models. In: 14th Conf. On Wea. Analysis and Forecasting, Amer. Meteor. Soc. pp. 34–41.

Heideman, K.F., Fritsch, J.M., 1988. Forcing mechanisms and other characteristics of significant summertime precipitation. Weather Forecast. 3, 115–130.

Huang, L., Meng, Z., 2014. Quality of the target area for metrics with different non-linearities in a mesoscale convective system. Mon. Weather Rev. 142, 2379–2397.

Huang, S., Li, Z., Bao, C., 1986. Heavy Rains in the First Rainy Season of South China (in Chinese). Guangdong Science and Technology Press, pp. 230.

Huang, Y., Liu, Y., Liu, Y., Li, H., Knievel, J.C., 2019a. Mechanisms for a record-breaking rainfall in the coastal metropolitan city of Guangzhou, China: observation analysis and nested very large eddy simulation with the WRF Model. J. Geophys. Res. 124, 1370–1391. https://doi.org/10.1029/2018JD029668.

Huang, Y., Liu, Y., Liu, Y., Li, H., Knievel, J.C., 2019b. Budget analyses of a record-breaking rainfall event in the coastal metropolitan city of Guangzhou, China. J. Geophys. Res. https://doi.org/10.1029/2018JD030229. in press.

Huffman, G.J., et al., 2007. The TRMM Multi-satellite Precipitation Analysis (TMPA): quasi-global, multiyear, combined-sensor precipitation estimates at fine scales. Hydrometeor 8, 38–55.

Jiang, Z., Zhang, D.L., Xia, R., Qian, T., 2017. Diurnal variations of presummer rainfall over southern China. J. Clim. 30, 755–773. https://doi.org/10.1175/JCLI-D-15-0666.1.

Johnson, A., et al., 2014. Multiscale characteristics and evolution of perturbations for warm season convection allowing precipitation forecasts: dependence on background flow and method of perturbation. Mon. Weather Rev. 142, 1053–1073. https://doi.org/10.1175/MWR-D-13-00204.1.

Junker, N.W., Schneider, R.S., Fauver, S.L., 1999. A study of heavy precipitation events during the Great Midwest Flood of 1993. Weather Forecast. 14, 701–712.

Kuo, Y., Chen, G.T.-J., 1990. The Taiwan area mesoscale experiment (TAMEX): an overview. Bull. Amer. Meteor. Soc. 71, 488–503.

Liu, X., Luo, Y., Guan, Z., Zhang, D.L., 2018. An extreme rainfall event in coastal South China during SCMREX-2014: formation and roles of rainband and echo trainings. J. Geophys. Res. 123, 9256–9278. https://doi.org/10.1029/2018JD028418.

Luo, Y., Wang, H., Zhang, R., 2013. Comparison of rainfall characteristics and convective properties of monsoon precipitation systems over South China and the Yangtze and Huai river basin. J. Clim. 26, 110–132.

Luo, Y., Wu, M., Ren, F., Li, J., Wong, W., 2016. Synoptic situations of extreme hourly precipitation over China. J. Clim. 29, 8703–8719. https://doi.org/10.1175/JCLI-D-16-0057.1.

Maddox, R.A., Chappell, C.F., Hoxit, L.R., 1979. Synoptic and meso-α-scale aspects of flash flood events. Bull. Amer. Meteor. Soc. 60, 115–123.

Matsumoto, S., 1971. Characteristic feature of Baiu front associated with heavy precipitation. J. Meteorol. Soc. Jpn 49, 267–281.

Melhauser, C., Zhang, F., 2012. Practical and intrinsic predictability of severe and convective weather at the mesoscales. J. Atmos. Sci. 69, 3350–3371.

Mohan, P.R., Srinivas, C.V., Yesubabu, V., Baskaran, R., Venkatraman, B., 2018. Simulation of a heavy rainfall event over Chennai in Southeast India using WRF: sensitivity to microphysics parameterization. Atmos. Res. 210, 83–99.

Moore, J.T., Glass, F.H., Graves, C.E., Rochette, S.M., Singer, M.J., 2003. The environment of warm-season elevated thunderstorms associated with heavy precipitation over the Central United States. Weather Forecast. 18, 861–878.

Nielsen, E.R., Schumacher, R.S., 2016. Using Convection-Allowing Ensembles to Understand the Predictability of an Extreme Rainfall Event. Mon. Wea. Rev. 144, 3651–3676. https://doi.org/10.1175/MWR-D-16-0083.1.

Ninomiya, K., 1984. Characteristics of the Baiu front as a predominant subtropical front in the summer northern hemisphere. J. Meteorol. Soc. Jpn 62, 880–894.

Ninomiya, K., 2000. Large and meso-α-scale characteristics of Meiyu/Baiu front associated with intense rainfalls in 1–10 July1991. J. Meteorol. Soc. Jpn 78, 141–157.

Nitta, T., Sekine, S., 1994. Diurnal-variation of convective activity over the tropical western Pacific. J. Meteorol. Soc. Jpn 72, 627–641.

Patade, S., Kulkarni, G., Patade, S., Deshmukh, A., Dangat, P., Axisa, D., Fan, J.W., Pradeepkumar, P., Prabha, T.V., 2019. Role of liquid phase in the development of ice phase in monsoon clouds: aircraft observations and numerical simulations. Atmos. Res. 229, 157–174.

Schumacher, R.S., Davis, C.A., 2010. Ensemble-based forecast uncertainty analysis of diverse heavy rainfall events. Weather Forecast. 25, 1103–1122.

Schumacher, R.S., Johnson, R.H., 2005. Organization and environmental properties of extreme-rain-producing mesoscale convective systems. Mon. Weather Rev. 133, 961–976.

Sharma, K., 2016. Forecasting of monsoon heavy rains: challenges in NWP. In: SPIE Asia-Pacific Remote Sensing, 98821O.

Srinivas, C.V., Yesubabu, V., Prasad, D.H., Prasad, K., Greeshma, M.M., Baskaran, R., Venkatraman, B., 2018. Simulation of an extreme heavy rainfall event over Chennai, India using WRF: sensitivity to grid resolution and boundary layer physics. Atmos. Res. 210, 66–82.

Tao, S., Chen, L., 1987. A review of recent research on the East Asian summer monsoon in China. In: Chang, C.-P., Krishnamurti, T.N. (Eds.), Monsoon Meteorology. Oxford Univ. Press, New York, pp. 60–92.

Terao, T., Islam, M.N., Hayashi, T., Oka, T., 2006. Nocturnal jet and its effects on early morning rainfall peak over northeastern Bangladesh during the summer monsoon season. Geophys. Res. Lett. 33, L18806.

Wang, H., Luo, Y., Jou, J.D., 2014. Initiation, maintenance, and properties of convection in an extreme rainfall event during SCMREX: observational analysis. J. Geophys. Res. Atmos. 119, 13,206–13,232.

Wang, J., Feng, J., Yan, Z., 2015. Potential sensitivity of warm season precipitation to urbanization extents: modeling study in Beijing-Tianjin-Hebei urban agglomeration in China. J. Geophys. Res. Atmos. 120, 9408–9425.

Wu, M., Luo, Y., 2016. Mesoscale observational analysis of lifting mechanism of a warm-sector convective system producing the maximal daily precipitation in China mainland during pre-summer rainy season of 2015. J. Meteorol. Res. 30, 719–736.

Wu, M., Luo, Y., Chen, F., Wong, W.K., 2019. Observed link of extreme hourly precipitation changes to urbanization over coastal South China. J. Appl. Meteorol. Climatol. 58, 1799–1819. https://doi.org/10.1175/JAMC-D-18-0284.1.

Xia, R., Zhao, S., Sun, J., 2006. Analysis and study on environment characteristics of the Class-1 β mesoscale system in the warm sector ahead of front in South China (in Chinese). Atmos. Sci. 30, 988–1007.

Xu, W., Zipser, E.J., Liu, C., 2009. Rainfall characteristics and convective properties of mei-yu precipitation systems over South China, Taiwan, and the South China Sea. Part I: TRMM observations. Mon. Weather Rev. 137, 4261–4275.

Xu, W., Zipser, E.J., Chen, Y., Liu, C., Liou, Y.C., Lee, W.C., Jou, B.J.D., 2012. An orography-associated extreme rainfall event during TiMREX: initiation, storm evolution, and maintenance. Mon. Weather Rev. 140, 2555–2574.

Zhang, C., Uyeda, H., Yamada, H., et al., 2006. Characteristics of mesoscale convective systems over the east part of continental China during the Meiyu from 2001 to 2003. J. Meteorol. Soc. Jpn 84, 763–782.

Zhang, X., Meng, W., Zhang, Y., et al., 2011. Analysis of mesoscale convective systems associated with a warm-sector heavy rains event over South China. J. Trop. Meteorol. 17, 1–10.

Zhou, T., Yu, R., Chen, H., Dai, A., Pan, Y., 2008. Summer Precipitation Frequency, Intensity, and Diurnal Cycle over China: a comparison of satellite data with rain gauge observations. J. Clim. 21 (16), 3997–4010.

Zhu, L., Meng, Z., Zhang, F., et al., 2017. The influence of sea-and land-breeze circulations on the diurnal variability of precipitation over a tropical island. Atmos. Chem. Phys. 17, 13213–13232.